JOURNAL OF GEOPHYSICAL RESEARCH, VOL. 85, NO. A9, PAGES 4642–4652, SEPTEMBER 1, 1980

Negative Ion Chemistry in the Terrestrial *D* Region and Signal Flow Graph Theory

J. WISEMBERG AND G. KOCKARTS

Institut d'Aéronomie Spatiale, B-1180 Bruxelles, Belgium

Aeronomic systems such as the negative ion chemistry in the *D* region are characterized by numerous reactions involving positive, negative, and neutral species. Classical solutions of such systems do not necessarily point out the role played by each parameter. When the chemical system is considered as a graph, it is possible to apply the signal flow graph technique, which allows a quantitative evaluation of the various paths and loops. A negative ion model is obtained for daytime conditions by using the signal flow graph technique, which is briefly described. This reference model is analyzed in terms of transmittances, path gains, and loop gains. An arbitrary variation of atomic oxygen and nitric oxide is introduced at a height of 65 km in order to show the induced effects on the negative ions and on the electron concentrations. Variations of the ratio λ between negative ions and electrons are also presented.

1. INTRODUCTION

Mass spectrometer observations [e.g., *Narcisi and Bailey*, 1965; *Narcisi*, 1967; *Goldberg and Blumle*, 1970; *Narcisi et al.*, 1971, 1972; *Arnold et al.*, 1971; *Goldberg and Aikin*, 1971; *Johannessen and Krankowsky*, 1972; *Zbinden et al.*, 1974, 1975] have shown that the terrestrial *D* region is characterized by many positive and negative ions which result from external ionization processes leading initially to electrons, molecular oxygen, nitrogen, and nitric oxide positive ions. Heavy negative ions [*Arnold and Henschen*, 1978] as well as positive ions [*Arijs et al.*, 1978; *Arnold et al.*, 1978] have also been detected in the stratosphere with balloon-borne mass spectrometers.

Prior to any direct determination of negative ions in the *D* region, *Reid* [1964] showed that it is unlikely for O_2^- to be the dominant negative ion, although its formation is rather easy by electron attachment to atmospheric molecular oxygen. This ion is actually an initial step in a long chain of reactions which has been investigated in recent years for understanding of negative ion chemistry in the terrestrial atmosphere [e.g., *Turco and Sechrist*, 1972*a*, *b*; *Thomas et al.*, 1973*a*, *b*; *Thomas*, 1974; *Turco*, 1974; *Ferguson*, 1974; *Reid*, 1976; *Swider*, 1977]. Approximately 60 chemical reactions are at the present time involved in the negative ion chemistry of the *D* region, and this number does not account for possible negative cluster formation. A similar situation occurs for the positive ions, leading to a total of the order of 120 chemical reactions. Comparisons between various theoretical models is not always easy, since they usually differ not only by the adopted reaction scheme and the corresponding reaction rates but also by the model of the neutral minor constituents involved in various production and loss processes. When the neutral model and some poorly known reaction rates are considered as variable parameters, it appears that the ion chemistry of the *D* region readily becomes a 'black box' from which it is difficult to extract quantitative information regarding a specific parameter. In a system with a few reactions, a knowledge of the reaction rates and the neutral concentrations leads rather easily to a determination of the most important mechanisms. But in large systems, cycling processes and feedback mechanisms make such an analysis more difficult.

The purpose of the present paper is to introduce a new way to analyze *D* region ion chemistry by considering the large chemical system as a signal flow graph. Such a technique, summarized in Appendix A, gives direct access to the black box by assigning quantitative values to any path or loop in the system and by showing quantitatively how any input to the system is transmitted along the various paths. Comparisons with in situ measurements are left out for future work.

A daytime neutral model atmosphere as well as ion reaction rates and electron-ion pair production rates are presented in section 2. The signal flow graph technique is then applied to the negative ion chemistry in section 3, which also contains a discussion of some computational problems associated with the steady state solution. An oversimplified example is given in Appendix B in order to clarify the signal flow graph technique and to show the identity with a classical solution, which is, however, unable to give the same amount of physical information on the whole system. A reference model for the negative ions is presented in section 4 in terms of electron and ion concentrations, production, and loss rate. The importance of various reaction paths is discussed as a function of height. Using the reference model, a parametric analysis is made at 65-km altitude in section 5. Such an analysis indicates how variations of the neutral model can lead to different negative ion concentrations without any change of the adopted reaction rates. Finally, the potential contribution of signal flow graph technique is summarized in the last section.

2. RATE COEFFICIENTS, NEUTRAL MODEL, AND ELECTRON-ION PAIR PRODUCTION

When electrons are produced in the *D* region between the stratopause and the mesopause, a negative ion chemistry chain is initiated by attachment with major atmospheric neutral constituents and with ozone according to the following processes:

$$e + O_2 + O_2 \rightarrow O_2^- + O_2 \qquad k_1 = 4 \times 10^{-30} \exp(-193/T) \quad (1)$$

$$e + O_2 + N_2 \rightarrow O_2^- + N_2 \qquad k_2 = 1 \times 10^{-31} \quad (2)$$

$$e + O_3 \rightarrow O^- + O_2 \qquad k_3 = 9.1 \times 10^{-12} (T/300)^{1.46} \quad (3)$$

where the reaction rate k_1 in $cm^6\ s^{-1}$ is measured as a function of the temperature T by *Truby* [1972], k_2 in $cm^6\ s^{-1}$ is given by *Phelps* [1969], and k_3 in $cm^3\ s^{-1}$ is measured by *Stelman et al.* [1972]. A schematic diagram of negative ion reactions based on *Ferguson*'s [1974] analysis is given in Figure 1. The dia-

Paper number 80A0508.
0148-0227/80/080A-0508$01.00

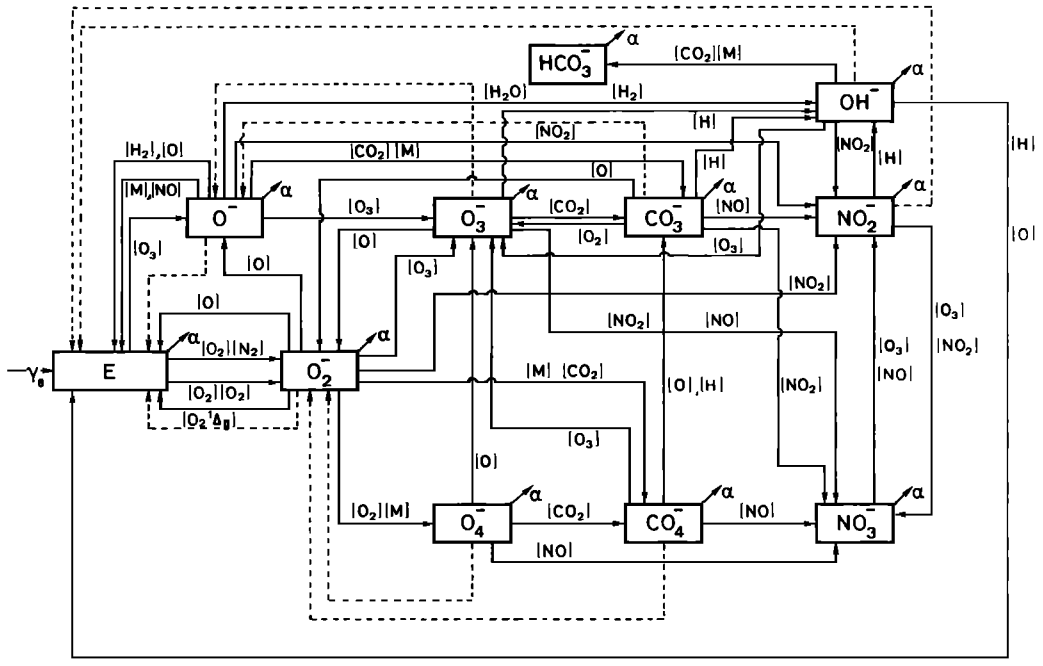

Fig. 1. Schematic diagram of negative ion reactions in the daytime D region. Neutral constituents involved in the reactions are indicated in brackets. Dashed lines correspond to photodestruction processes. Arrows labeled α correspond to dissociative recombination for electrons and to mutual neutralization for negative ions. The external production leading to electrons E and to positive ions is indicated by γ_e (cm^{-3} s^{-1}).

gram includes photodestruction processes with coefficients J, in units per second, since emphasis will be given to daytime negative chemistry. The neutral reactants, M being the total concentration, are indicated on each edge joining two negative ions. The hydration effects on the negative ions are neglected in Figure 1 [*Ferguson*, 1974], although *Keesee et al.* [1979] conclude that hydrates of CO_3^-, HCO_3^-, and NO_3^- should be prevalent in the nighttime lower ionosphere, which is not considered in the present paper. The reaction rate coefficients corresponding to Figure 1 are given in Table 1, which contains only measured values compiled by *Albritton* [1978]. These rate constants correspond to a temperature of the order of 300 K, and no attempt will be made here to introduce temperature dependences. Negative ions and electrons are also subject to recombination with positive ions. For any negative ion X^- a recombination coefficient α_1 with any positive ion Y^+ is adopted from *D. Smith et al.* [1976] such that

$$X^- + Y^+ \rightarrow \text{neutrals} \qquad \alpha_1 = 6 \times 10^{-8}\ \text{cm}^3\ \text{s}^{-1} \qquad (4)$$

The dissociative recombination coefficients for O_2^+ and NO^+ are taken from *Mul and McGowan* [1979]:

$$e + O_2^+ \rightarrow \text{neutrals} \qquad \alpha_2 = 1.9 \times 10^{-7}\,(300/T)^{0.5}\ \text{cm}^3\ \text{s}^{-1} \qquad (5)$$

and

$$e + NO^+ \rightarrow \text{neutrals} \qquad \alpha_3 = 2.3 \times 10^{-7}\,(300/T)^{0.5}\ \text{cm}^3\ \text{s}^{-1} \qquad (6)$$

The recombination rate coefficient of electrons with other positive ions such as clusters is adopted as

$$e + Y^+ \rightarrow \text{neutrals} \qquad \alpha_4 = 3 \times 10^{-6}\ \text{cm}^3\ \text{s}^{-1} \qquad (7)$$

in agreement with the values of *Huang et al.* [1978] for water cluster ions. Photodestruction cross sections have been measured and summarized by *G. P. Smith et al.* [1978] and by *Lee and Smith* [1979]. By using these cross sections and the solar fluxes of *Smith and Gottlieb* [1974] the following photodetachment rates are obtained: $J_{O^-} = 1.4\ s^{-1}$, $J_{O_2^-} = 0.38\ s^{-1}$, $J_{OH^-} = 1.1\ s^{-1}$, and $J_{NO_2^-} = 8 \times 10^{-4}\ s^{-1}$. The photodissociation of CO_3^- leads to O^- and CO_2 with a rate $J_{CO_3^-} = 0.15\ s^{-1}$, whereas the photodissociation of O_3^- leads to O^- and O_2 with a rate $J_{O_3^-} = 0.47\ s^{-1}$. The photodissociation cross section of O_3^- is, however, characterized by a fine structure which requires further studies [*Lee and Smith*, 1979]. Photodestruction of CO_4^- and O_4^- are assumed to give O_2^- with rates of $J_{CO_4^-} = 6.2 \times 10^{-3}\ s^{-1}$ and $J_{O_4^-} = 0.24\ s^{-1}$, although *Cosby et al.* [1976] are not excluding photodetachment. At the present time the branching ratio between photodetachment and photodissociation is, however, not known. According to *Cosby et al.* [1976], HCO_3^- apparently neither photodetaches or photodissociates for wavelengths above 458 nm. Since the electron affinity of NO_3^- is 3.9 ± 0.2 eV [*Ferguson et al.*, 1972], no photodetachment mechanism for this ion is introduced in the present work. The negative ion system corresponds therefore to 44 ion neutral reactions given in Table 1, to three attachment processes given by equations (1) to (3), and to eight photodestruction processes. The coupling between the negative ions and the positive ions occurs through reactions (4) to (6), which imply a knowledge of the positive ion concentrations.

Instead of fulfilling the condition of electroneutrality with a fictitious positive ion Y^+, individual positive ions are computed with the measured reaction rates [*Albritton*, 1978; *Ferguson*, 1974] given in Table 2 without any temperature dependence. The sole significant photodissociation coefficient for positive clusters is computed for $O_2^+ \cdot H_2O$ with the cross sections of *Smith and Lee* [1978], and it leads to a value $J_{O_2^+ \cdot H_2O} = 0.42\ s^{-1}$. The introduction of a detailed positive ionic model is made to account for a possible simultaneous effect of certain parameters on the positive and negative ion chemistry. Such an effect could lead to a nonlinear coupling between positive and negative systems.

The neutral concentrations involved in Table 1 and in

TABLE 1. Negative Ion Reaction Rates*

Reaction	Rate
$O_2^- + O \rightarrow e + O_3$	1.5(−10)†
$O_2^- + O_2(^1\Delta_g) \rightarrow e + O_2 + O_2$	2.0(−10)
$O_2^- + CO_2 + M \rightarrow CO_4^- + M$	4.7(−29)
$O_2^- + O_3 \rightarrow O_3^- + O_2$	6.0(−10)
$O_2^- + NO_2 \rightarrow NO_2^- + O_2$	7.0(−10)
$O_2^- + O \rightarrow O^- + O_2$	1.5(−10)
$O_2^- + O_2 + M \rightarrow O_4^- + M$	3.4(−31)‡
$O^- + O_2(^1\Delta_g) \rightarrow e + O_3$	3.0(−10)
$O^- + M \rightarrow e +$ neutrals	1.0(−12)
$O^- + O_3 \rightarrow O_3^- + O$	8.0(−10)
$O^- + H_2 \rightarrow e + H_2O$	5.8(−10)
$O^- + H_2 \rightarrow OH^- + H$	6.0(−11)
$O^- + O \rightarrow e + O_2$	1.9(−10)
$O^- + NO \rightarrow e + NO_2$	2.1(−10)
$O^- + CO_2 + M \rightarrow CO_3^- + M$	2.0(−28)
$O^- + NO_2 \rightarrow NO_2^- + O$	1.0(−9)
$O^- + H_2O \rightarrow OH^- + OH$	6.0(−13)
$O_4^- + O \rightarrow O_3^- + O_2$	4.0(−10)
$O_4^- + NO \rightarrow NO_3^- + O_2$	2.5(−10)
$O_4^- + CO_2 \rightarrow CO_4^- + O_2$	4.3(−10)
$O_3^- + O \rightarrow O_2^- + O_2$	2.5(−10)
$O_3^- + NO \rightarrow NO_3^- + O$	2.6(−12)
$O_3^- + CO_2 \rightarrow CO_3^- + O_2$	5.5(−10)
$O_3^- + NO_2 \rightarrow NO_3^- + O_2$	2.8(−10)
$O_3^- + H \rightarrow OH^- + O_2$	8.4(−10)
$CO_4^- + NO \rightarrow NO_3^- + CO_2$	4.8(−11)
$CO_4^- + O \rightarrow CO_3^- + O_2$	1.4(−10)
$CO_4^- + O_3 \rightarrow O_3^- + CO_2 + O_2$	1.3(−10)
$CO_4^- + H \rightarrow CO_3^- + OH$	2.2(−10)
$NO_3^- + O_3 \rightarrow NO_2^- + O_2 + O_2$	1.0(−13)
$NO_3^- + NO \rightarrow NO_2^- + NO_2$	1.0(−12)
$NO_2^- + H \rightarrow OH^- + NO$	3.0(−10)
$NO_2^- + O_3 \rightarrow NO_3^- + O_2$	1.2(−10)
$NO_2^- + NO_2 \rightarrow NO_3^- + NO$	2.0(−13)
$OH^- + H \rightarrow e + H_2O$	1.4(−9)
$OH^- + O_3 \rightarrow O_3^- + OH$	9.0(−10)
$OH^- + O \rightarrow e + HO_2$	2.0(−10)
$OH^- + NO_2 \rightarrow NO_2^- + OH$	1.1(−9)
$OH^- + CO_2 + O_2 \rightarrow HCO_3^- + O_2$	7.6(−28)
$CO_3^- + O \rightarrow O_2^- + CO_2$	1.1(−10)
$CO_3^- + NO_2 \rightarrow NO_3^- + CO_2$	2.0(−10)
$CO_3^- + NO \rightarrow NO_2^- + CO_2$	1.1(−11)
$CO_3^- + O_2 \rightarrow O_3^- + CO_2$	6.0(−15)
$CO_3^- + H \rightarrow OH^- + CO_2$	1.7(−10)

*From *Albritton* [1978]. Two-body rates are in $cm^3\ s^{-1}$; three-body rates are in $cm^6\ s^{-1}$.
†For 1.5(−10), read 1.5×10^{-10}.
‡Measured with M = He.

Table 2 are taken from the U.S. Standard Atmosphere (1976) for noon conditions at 45°N latitude. Such a model is similar to the recent mesospheric model developed by *Keneshea et al.* [1979]. Since NO and NO_2 concentrations are not given in this model, we adopt the high daytime values computed by *Turco and Sechrist* [1970, 1972*b*]. Vertical profiles of minor constituents used in our negative ionic reference model are summarized in Figure 2. Finally, the electron-ion pair productions used in the computations are shown in Figure 3. The quantities given in Figures 2 and 3 are variable, but they are adopted here as reference values. The effect of possible variations of atomic oxygen and nitric oxide will be described in section 5 as an application of the signal flow graph technique. This technique is presented in the following two sections for the negative ion model resulting from the reaction scheme, the electron-ion pair production, and the neutral model just described.

3. Signal Flow Graph Technique and Ion Chemistry

The ionic scheme given in Figure 1 has all the characteristics of the signal flow graph described in Appendix A. The various negative ionic species are nodes of the graph. Two consecutive nodes are joined by an edge indicating which neutral constituent is involved in the transformation, and successive edges form a path which can become a loop when the initial and final negative ions are identical. The input γ_e to the system represents the electron-ion pair production. Under equilibrium conditions between k types of negative ions including electrons, equation (B3) of Appendix B reduces to

$$P_i = T_{(i\leftarrow 1)} \times \gamma_e \tag{8}$$

where P_i is the production rate ($cm^{-3}\ s^{-1}$) of the i type ion and $T_{(i\leftarrow 1)}$ is the transmittance given by

$$T_{(i\leftarrow 1)} = \sum_{l=1}^{n} g_l \Delta_l / \Delta \tag{9}$$

In (9), n is the number of paths leading from the sole input 1 to the i type ion. The path gains g_l, and the amplification factors Δ_l/Δ are given by *Mason*'s [1956] rules described in Ap-

TABLE 2. Positive Ion Reaction Rates*

Reaction	Rate
$N_2^+ + O \rightarrow NO^+ + N$	1.4(−10)†
$N_2^+ + O_2 \rightarrow O_2^+ + N_2$	4.3(−11)
$O_2^+ + N_2 + N_2 \rightarrow O_2^+ \cdot N_2 + N_2$	8.0(−31)
$O_2^+ + H_2O + N_2 \rightarrow O_2^+ \cdot H_2O + N_2$	2.8(−28)
$O_2^+ + H_2O + O_2 \rightarrow O_2^+ \cdot H_2O + O_2$	2.3(−28)
$O_2^+ + NO \rightarrow NO^+ + O_2$	4.4(−10)
$O_2^+ + O_2 + O_2 \rightarrow O_4^+ + O_2$	2.5(−30)
$O_2^+ \cdot N_2 + H_2O \rightarrow O_2^+ \cdot H_2O + N_2$	4.0(−9)
$O_2^+ \cdot N_2 + N_2 \rightarrow O_2^+ + N_2 + N_2$	2.0(−11)
$O_2^+ \cdot N_2 + O_2 \rightarrow O_4^+ + N_2$	5.0(−11)
$O_4^+ + H_2O \rightarrow O_2^+ \cdot H_2O + O_2$	1.8(−9)
$O_4^+ + O \rightarrow O_2^+ + O_3$	3.0(−10)
$O_4^+ + O_2 \rightarrow O_2^+ + O_2 + O_2$	1.8(−13)
$O_2^+ \cdot H_2O + H_2O \rightarrow H_3O^+ + OH + O_2$	2.4(−10)
$O_2^+ \cdot H_2O + H_2O \rightarrow H_3O^+ \cdot OH + O_2$	1.4(−9)
$H_3O^+ + H_2O + M \rightarrow H_3O^+ \cdot H_2O + M$	7.0(−28)
$H_3O^+ \cdot OH + H_2O \rightarrow H_3O^+ \cdot H_2O + OH$	2.0(−9)
$H_3O^+ \cdot H_2O + H_2O + M \rightarrow H_3O^+ \cdot 2H_2O + M$	2.0(−27)
$H_3O^+ \cdot 2H_2O + H_2O + M \rightarrow H_3O^+ \cdot 3H_2O + M$	2.0(−27)
$H_3O^+ \cdot 3H_2O + M \rightarrow H_3O^+ \cdot 2H_2O + H_2O + M$	4.0(−15)
$H_3O^+ \cdot 3H_2O + H_2O + M \rightarrow H_3O^+ \cdot 4H_2O + M$	1.0(−29)
$H_3O^+ \cdot 4H_2O + M \rightarrow H_3O^+ \cdot 3H_2O + H_2O + M$	4.0(−15)
$NO^+ + N_2 + N_2 \rightarrow NO^+ \cdot N_2 + N_2$	1.5(−30)
$NO^+ + H_2O + M \rightarrow NO^+ \cdot H_2O + M$	1.3(−28)
$NO^+ + CO_2 + M \rightarrow NO^+ \cdot CO_2 + M$	5.0(−29)
$NO^+ \cdot CO_2 + H_2O \rightarrow NO^+ \cdot H_2O + CO_2$	1.0(−9)
$NO^+ \cdot H_2O + H \rightarrow H_3O^+ + NO$	7.0(−12)
$NO^+ \cdot H_2O + OH \rightarrow H_3O^+ + NO_2$	1.0(−10)
$NO^+ \cdot H_2O + H_2O + M \rightarrow NO^+ \cdot 2H_2O + M$	9.0(−28)
$NO^+ \cdot 2H_2O + H_2O + M \rightarrow NO^+ \cdot 3H_2O + M$	1.0(−27)
$NO^+ \cdot 2H_2O + M \rightarrow NO^+ \cdot H_2O + H_2O + M$	1.5(−14)
$NO^+ \cdot 3H_2O + M \rightarrow NO^+ \cdot 2H_2O + H_2O + M$	1.0(−12)
$NO^+ \cdot 3H_2O + H_2O \rightarrow H_3O^+ \cdot 2H_2O + HNO_2$	7.5(−11)
$NO^+ \cdot N_2 + CO_2 \rightarrow NO^+ \cdot CO_2 + N_2$	1.0(−9)‡

*From *Albritton* [1978]. Two-body rates are in $cm^3\ s^{-1}$; three-body rates are in $cm^6\ s^{-1}$.
†For 1.4(−10), read 1.4×10^{-10}.
‡See *Ferguson* [1974].

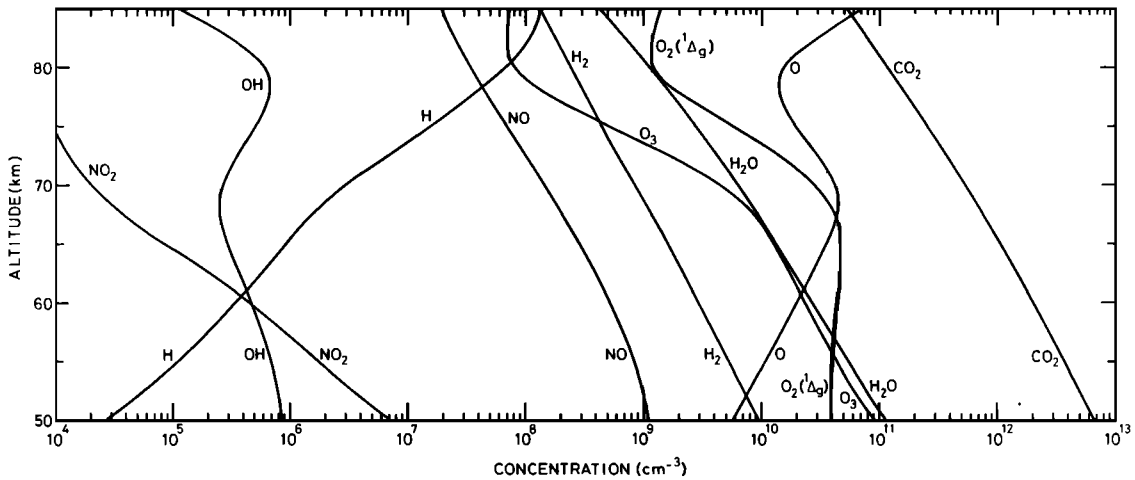

Fig. 2. Vertical profiles of neutral minor constituents involved in *D* region ion chemistry. Noontime conditions at 45°N latitude.

pendix A and applied to an oversimplified example in Appendix B. Computation of the production rates P_i by (8) leads immediately to the concentrations n_i, since

$$n_i = P_i/L_i \tag{10}$$

where L_i is the total loss rate in units per second of the i type ion. It is shown in Appendix B that the total loss rates L_i are simultaneously computed with the path gains g_l.

Mason's [1956] rules are strictly valid for linear systems of equations. Mutual neutralization between negative and positive ions as well as dissociative recombination between electron and positive ions can a priori introduce some nonlinearity, since the positive ions are not necessarily known. Such a nonlinearity can be removed with the help of the electroneutrality condition. Starting with two arbitrary relative distributions of n positive ions with relative concentration x_i^+ and m negative ions (including electrons) with relative concentration x_j^- such that

$$\sum_{i=1}^{n} x_i^+ = \sum_{j=1}^{m} x_j^- = 1 \tag{11}$$

it is possible to calculate an effective recombination coefficient

$$\alpha_{\text{eff}} = \sum_{i=1}^{n} \sum_{j=1}^{m} \alpha_{ij} x_i^+ x_j^- \tag{12}$$

where the recombination coefficients are given by (4) to (7). The corresponding total positive or negative concentration n_t is then

$$n_t = (\gamma_e/\alpha_{\text{eff}})^{1/2} \tag{13}$$

where γ_e is the input production rate. An initial set of positive and negative ions is obtained from the relations

$$n_i^+ = x_i^+ \times n_t \tag{14}$$

and

$$n_j^- = x_j^- \times n_t \tag{15}$$

The set of positive ions is used for a solution of the negative ion system, and the resulting negative ions are used to compute a new set of relative distributions x_j^-. The same procedure is used for the positive ions, and the iteration scheme (11) to (15) is repeated until convergence is reached. Convergence within 1% is obtained after three iterations.

Before solving the negative or positive ion system it is necessary to make a computer search of the various paths leading to a specific ion from the input γ_e. This can be done by associating a logical square matrix to the graph. The number of rows and columns of this matrix is equal to the number of nodes of the graph. An element (i, j) of this matrix is set to 1 if the ith ion can lead to the jth ion. In such a way any value 1 in the ith row indicates that the ion associated with the corresponding jth column can be produced by the ith ion. All unitary values in the ith row indicate the 'descendants' of the ith ion, and all unitary values in the ith column give the 'ascendants' of the ith ion. An analysis of each column leads then to the various paths which are memorized only if the last node is an input node and if a path does not go twice through the same node. Loops are obtained by considering each node as an input. Care must be taken to avoid multiple counting of loops resulting from input nodes which belong to the same loop. The total number of paths in Figure 1 is 729, and O_4^- is produced by 12 paths, O_2^- by 12 paths, CO_4^- by 24 paths, O^- by 28 paths, CO_3^- by 32 paths, O_3^- by 44 paths, OH^- by 112 paths, NO_2^- by 142 paths, HCO_3^- by 156 paths, and NO_3^- by 167 paths, respectively. The absolute abundance of a specific

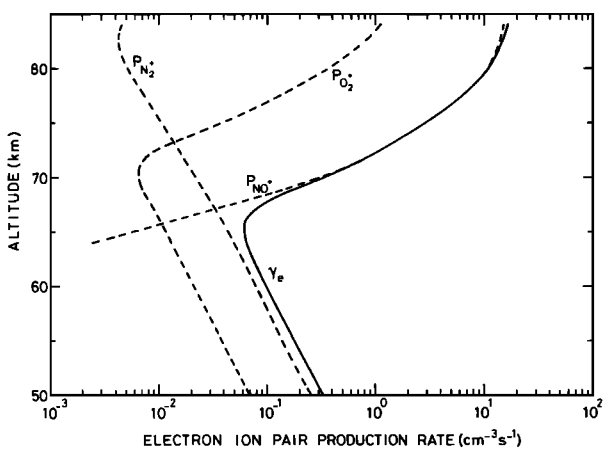

Fig. 3. Altitude dependence of the external electron production rate γ_e. Production rates of N_2^+, O_2^+, and NO^+ ions are also indicated.

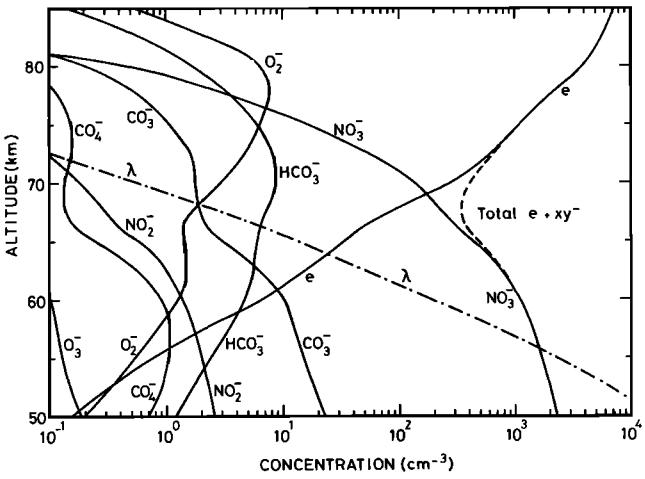

Fig. 4. Vertical profiles of negative ions and electrons. The ratio λ between the negative ion concentration and the electron concentration is given by the dotted-dashed lines, whereas the sum of the electron and negative ion concentration is given by the dashed line.

ion is not correlated with the number of paths. Expression (8) shows that the ion concentration is actually proportional to the transmittance, which depends on the path gains and the amplification factors.

The efficiency of the signal flow graph technique is particularly high for large systems where the great number of paths and loops makes it very difficult to find the most important mechanisms leading to a specific ion. In the numerical results of the next section we have neglected the paths which contribute by less than 1% to the transmittance from the input to each i type ion.

4. Analysis of the Reference Model for Negative Ions

The signal flow graph technique can be applied at any height in the D region as long as transport processes are negligible. The neutral model combined with the reaction rates and the electron production given in section 2 leads to the vertical profiles shown in Figure 4. Only the most important negative ions and the electron concentration are indicated. The dimensionless ratio λ between the total negative ion concentration and the electron concentration is given to show the height range where negative ions are more abundant than electrons. The ratio λ becomes equal to 1 near 69-km altitude. In the height range where negative ions are important, NO_3^- is always the most abundant ion, although CO_3^- and HCO_3^- are not completely negligible. This result is in contradiction with the model of *Thomas et al.* [1973*b*], where photodetachment was introduced as an important process, but it is in better agreement with the calculations of *Turco and Sechrist* [1972*a*, *b*]. Furthermore, the presence of HCO_3^- in Figure 4 is a direct consequence of its small loss rate by mutual neutralization with positive ions. Such differences are a direct consequence of the different neutral models, the different reaction schemes, and the different rate coefficients used in these ionic models. We will see in section 5 how variations in the neutral model modify the relative abundances of the major negative ions. At the present time the results of Figure 4 are considered as a reference model for which we want to show the type of information gained by the signal flow graph technique.

The initial electron production results from the input γ_e given in Figure 3, but electrons can be subsequently produced from other negative ions by photodetachment and by ion-neutral reactions. The importance of this effect is shown in Figure 5, which shows the electron production resulting from several negative ions. Figure 5 indicates that the transmittances reach values much larger than 1 when electron production resulting from a negative ion XY^- is greater than the input value γ_e. All curves or parts of curves to the right-hand side of the input γ_e correspond to amplification by chemical and photochemical processes such that the transmittance in (8) is greater than 1. At all heights below 82 km the electron production resulting from the negative ions is larger than the direct input production. Above 55-km altitude, O_2^- leads to the major electron production rate, although O_2^- is never a major negative ion in the region where negative ion concentrations are comparable to or greater than the electron concentration (see Figure 4). Figure 5 should not be interpreted as a mysterious electric charge creation resulting from the input γ_e, since the electron loss rates are always such that the electroneutrality condition is satisfied.

Negative ion production rates are shown in Figure 6 for the input γ_e of Figure 3. The production rates of negative ions are always equal to or greater than the electron production rates resulting from these ions, since mutual neutralization and photodissociation included in the transmittances leading to Figure 5 never lead to electron production. Furthermore, the losses of negative ions included in the transmittances leading to Figure 5 do not necessarily lead to electron production.

In our reference model, NO_3^- and CO_3^- and HCO_3^- are the major negative ions. The signal flow graph technique automatically allows a quantitative determination of the most important paths leading to these ions. Figure 7 shows the total production rates of NO_3^- and CO_3^- and the contribution of all paths leading to at least 1% of the total production. Each path is characterized by a number which is obtained by following the technique described in section 3, and the various paths are identified in Table 3. It appears that a path can be almost negligible in a certain height range and can become very important in another height range. The partial productions resulting from a specific path are not represented anymore in Figure 7 when they contribute less than 1% to the

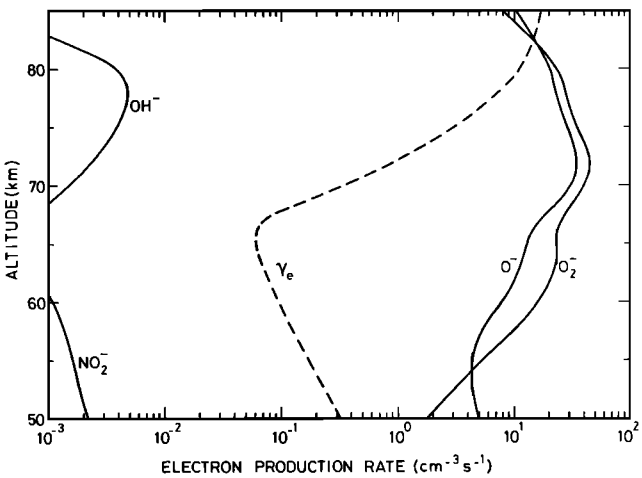

Fig. 5. Vertical distribution of the electron production rates resulting from photodetachment and collisional detachment of various negative ions. The dashed curve represents the external input γ_e of Figure 3.

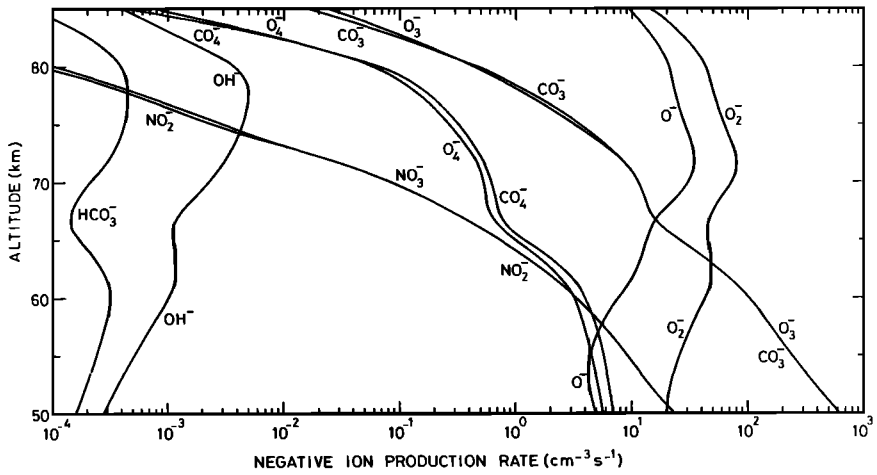

Fig. 6. Vertical distributions of various negative ion production rates for the external input γ_e of Figure 3.

total transmittance leading to this ion. Understanding of the negative ion chemistry can be completed by showing the loss rates (in units per second) as in Figure 8. The extremely high loss rate of O^- explains why the ion is not even shown in Figure 4. The effect of the high production rate of O_2^- (see Figure 6) is easily attenuated by its high loss rate shown in Figure 8. Furthermore, the fact that NO_3^- is the major negative ion in the reference model can now be understood, since its loss rate in Figure 8 is extremely small. As a consequence, a weak production path can significantly contribute to the buildup of NO_3^- ions. As an example, path 77 (see Figure 7 and Table 3), which represents only 9% of the NO_3^- production at 50 km, is the second production path (25%) above 60-km altitude. Furthermore, the O_4^- production by the reaction between O_2^- and O_2 is so small that it represents less than 2% of the total O_2^- loss at 65 km. A similar situation is found for path 68, which accounts for approximately 6% of the NO_3^- production at 65 km. The transitions from O_2^- to CO_4^- and from CO_4^- to NO_3^- both represent less than 1% of the total losses of O_2^- and CO_4^-, respectively. Such a situation could lead to the omission of path 77 or 68 if the signal flow graph technique had not been used, despite the fact that the cumulative production of the two paths represents approximately 30% of the NO_3^- production.

Finally, Figure 7 clearly indicates that above 60 km path 499 leads to practically all of the CO_3^- production and its extension (path 102) is responsible for the NO_3^- production, for which the loss rate is very small. As is pointed out in Appendix B, the relative losses along a specific path determine the path's absolute importance. Since atomic oxygen and nitric oxide influence the loss of CO_3^-, one can expect variations of these neutral constituents to play a role in negative ion production. This aspect is discussed in section 5.

At lower heights, around 50 km, other paths besides path 499 become significant. The most important reaction chains at 50 km are shown in Figure 9, which also gives the major paths at 60 km. The appearance of these new paths at 50 km is essentially a consequence of the increase in the neutral concentration which favors the reaction $O_2^- + O_2 + M \rightarrow O_4^- + M$ with respect to the reaction $O_2^- + O_3 \rightarrow O_3^- + O_2$. The situation for CO_4^- at 50 km is similar to that of CO_3^- at 60 km, since any increase in nitric oxide favors NO_3^- production. Furthermore, a decrease in ozone gives more importance to the paths going through CO_4^-. Finally, the feedback reactions from O_2^- to e (see Figure 1) largely depend on the concentrations in atomic oxygen and excited molecular oxygen $O_2(^1\Delta_g)$.

In summary, Figures 5 to 8, computed for an input γ_e, indicate the type of analysis which can be made with the signal

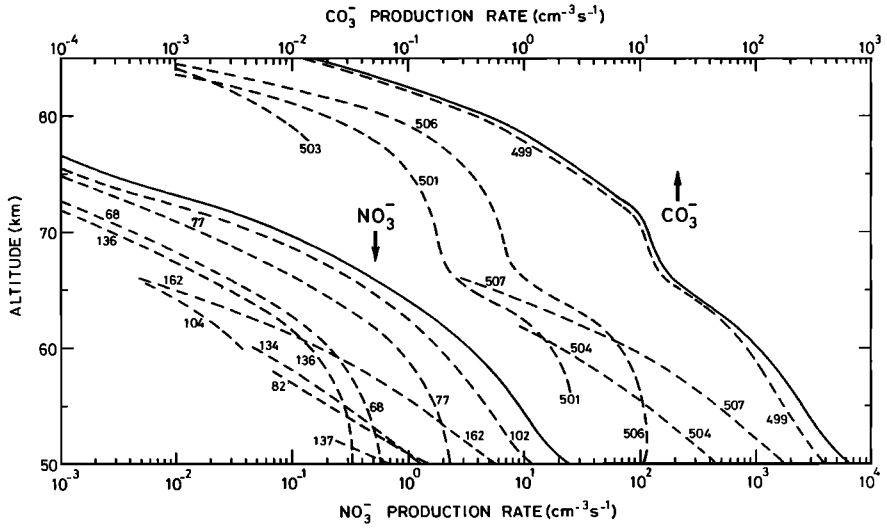

Fig. 7. Contribution of individual paths to NO_3^- and CO_3^- production rates. The paths are identified in Table 3.

TABLE 3. Paths Leading to NO_3^- and CO_3^- Ions

Path No.	Path
68	$e \rightarrow O_2^- \rightarrow CO_4^- \rightarrow NO_3^-$
77	$e \rightarrow O_2^- \rightarrow O_4^- \rightarrow CO_4^- \rightarrow NO_3^-$
82	$e \rightarrow O_2^- \rightarrow O_3^- \rightarrow CO_3^- \rightarrow NO_3^-$
102	$e \rightarrow O_2^- \rightarrow O_3^- \rightarrow CO_3^- \rightarrow NO_2^- \rightarrow NO_3^-$
104	$e \rightarrow O_2^- \rightarrow CO_4^- \rightarrow CO_3^- \rightarrow NO_2^- \rightarrow NO_3^-$
134	$e \rightarrow O_2^- \rightarrow CO_4^- \rightarrow O_3^- \rightarrow CO_3^- \rightarrow NO_2^- \rightarrow NO_3^-$
136	$e \rightarrow O_2^- \rightarrow O_4^- \rightarrow CO_4^- \rightarrow CO_3^- \rightarrow NO_2^- \rightarrow NO_3^-$
137	$e \rightarrow O_2^- \rightarrow O_4^- \rightarrow CO_4^- \rightarrow O_3^- \rightarrow CO_3^- \rightarrow NO_3^-$
162	$e \rightarrow O_2^- \rightarrow O_4^- \rightarrow CO_4^- \rightarrow O_3^- \rightarrow CO_3^- \rightarrow NO_2^- \rightarrow NO_3^-$
499	$e \rightarrow O_2^- \rightarrow O_3^- \rightarrow CO_3^-$
501	$e \rightarrow O_2^- \rightarrow CO_4^- \rightarrow CO_3^-$
503	$e \rightarrow O_2^- \rightarrow O_4^- \rightarrow O_3^- \rightarrow CO_3^-$
504	$e \rightarrow O_2^- \rightarrow CO_4^- \rightarrow O_3^- \rightarrow CO_3^-$
506	$e \rightarrow O_2^- \rightarrow O_4^- \rightarrow CO_4^- \rightarrow CO_3^-$
507	$e \rightarrow O_2^- \rightarrow O_4^- \rightarrow CO_4^- \rightarrow O_3^- \rightarrow CO_3^-$

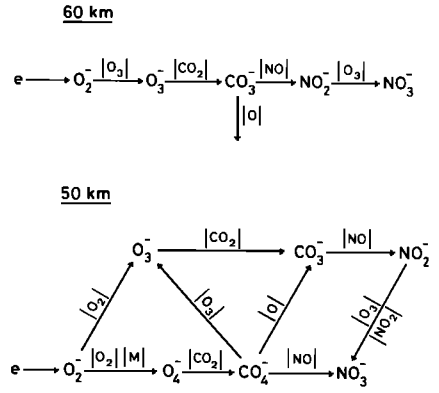

Fig. 9. Comparison of the reaction chains leading to NO_3^- at 60-km and 50-km altitude.

flow graph technique. Similar studies can be undertaken by considering reaction rates, photodetachment rates, or neutral concentrations as variable parameters. Since we used only measured rate coefficients [*Albritton*, 1978; *Ferguson*, 1974; *G. P. Smith et al.*, 1978; *D. Smith et al.*, 1976; *Truby*, 1972; *Phelps*, 1969; *Stelman et al.*, 1972; *Mul and McGowan*, 1979], we prefer to indicate in the following section the effect of variations in the neutral model which essentially results from theoretical computations [*Keneshea et al.*, 1979; *Turco and Sechrist*, 1970, 1972*b*]. This does not imply that the neutral models are unreliable, but variations of neutral minor constituents are real geophysical phenomena which can induce significant ionospheric modifications.

5. Effect of Variations of the Minor Neutral Constituents

It has been shown in the preceding section how the height variation of the neutral atmosphere can affect the paths leading to NO_3^- and CO_3^- ions. Nitric oxide, atomic oxygen, ozone, and excited molecular oxygen are of major importance in the evaluation of the transmittances associated with the predominant paths. It is therefore interesting to evaluate their effects at 65-km altitude, where NO_3^- is the major negative ion in the reference model. At 65-km altitude the neutral model adopted in section 2 leads to the following concentrations: $n(NO) = 2.9 \times 10^8$ cm^{-3}, $n(O) = 3.5 \times 10^{10}$ cm^{-3}, $n(O_3) = 1.3 \times 10^{10}$ cm^{-3}, and $n(O_2{}^1\Delta_g) = 4.6 \times 10^{10}$ cm^{-3}.

In an analysis of minor constituents in the middle atmosphere, *Ackerman* [1979] indicates that nitric oxide measurements at 65 km range between 10^7 cm^3 and 2×10^8 cm^{-3}. We adopt here an arbitrary variation from 10^7 cm^{-3} to 10^9 cm^{-3}. When all other parameters of the reference model are kept constant, such a variation leads to the results shown in the left part of Figure 10. It appears that an increase of NO at 65-km altitude leads to an increase of NO_3^- accompanied by a decrease of CO_3^-, of HCO_3^-, and of the electron concentration. The dimensionless ratio λ is also shown, and the vertical arrow corresponds to the nitric oxide concentration in the reference model. It is important to note that a variation of NO can lead to a significant change of the rate λ between negative ions and electrons. It should be noted that variations of NO at 65 km do not significantly modify the input γ_e of Figure 3, since at this altitude the electron-ion pair production essentially results from cosmic rays without Lyman α production of NO^+.

A detailed analysis of the nitric oxide effect is presented in Table 4. This table gives the total transmittance T_i and the total loss L of NO_3^- as a function of the nitric oxide concentration. Path gains g_i, amplification factors Δ_i/Δ, and partial transmittances T_i are given for several paths labeled i and shown in Table 3. The transmittances T_i are related by (8) to the production in Figure 7. The lines labeled $\%_i$ give the importance of path i in percents. It appears that the importance of a path changes as a function of the nitric oxide concentration but not in the same way as the corresponding path gain. As an example, path 82 has a path gain g_{82} unaffected by nit-

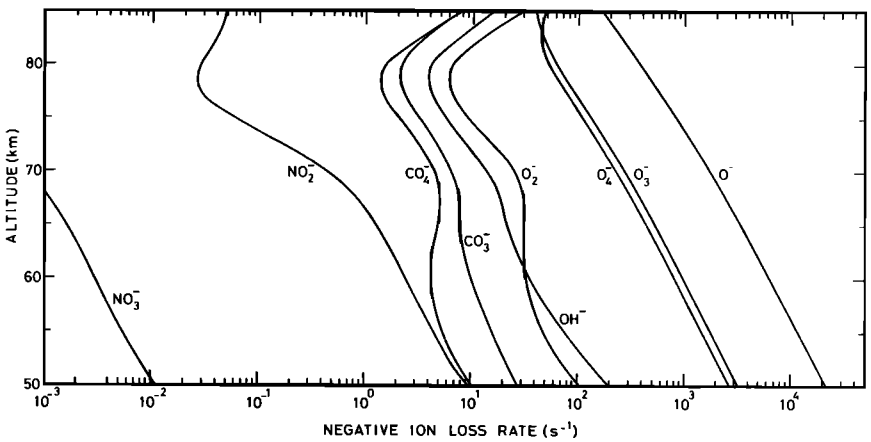

Fig. 8. Vertical profiles of some negative ion loss rates (s^{-1}) for the external input γ_e of Figure 3.

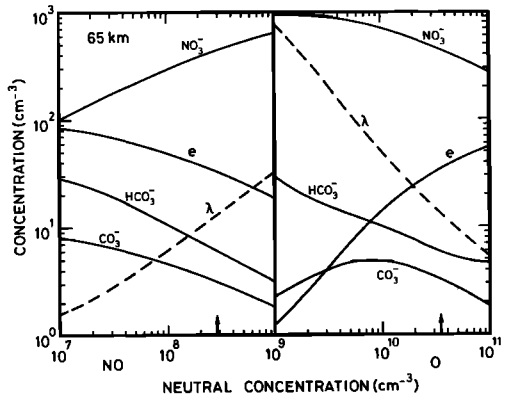

Fig. 10. Electron and negative ion concentrations at 65 km as a function (left) of nitric oxide concentration and (right) of atomic oxygen concentration. The dimensionless ratio λ is also shown. The vertical arrows indicate the NO and O concentrations used in the reference model of Figure 4.

ric oxide variations. But its amplification factor Δ_{82}/Δ decreases slowly with an increase of nitric oxide, and the partial transmittance T_{82} decreases in the same way as Δ_{82}/Δ. The two other paths 77 and 102 have path gains which increase with nitric oxide. In this case the decrease of the amplification factors Δ_{77}/Δ and Δ_{102}/Δ is not sufficient to prevent an increase of the partial transmittances T_{77} and T_{102}. As a result, the importance of path 82 strongly decreases when nitric oxide increases, and this path represents less than 1% of the total transmittance when the nitric oxide concentration reaches a value of 10^8 cm^{-3}.

A similar analysis made for CO_3^- indicates a decrease of the transmittance resulting from a decrease in the amplification factor of path 499 which always remains the most important path.

The right-hand part of Figure 10 shows the effect of a variation in atomic oxygen. Since O, O_3, and $O_2(^1\Delta_g)$ are not independent quantities in the neutral chemistry, variations of atomic oxygen are assumed to be accompanied by ozone and excited molecular oxygen such that the ratios $n(O_3)/n(O)$ and $n(O_2{}^1\Delta_g)/n(O_3)$ are identical to the values of the reference model as well as the nitric oxide concentration. Figure 10 shows that any increase in atomic oxygen produces an increase of the electron concentration and a subsequent decrease of the ratio λ. The concentrations of NO_3^- and HCO_3^- decrease when atomic oxygen increases. The maximum in CO_3^- concentration results from a competition between CO_3^- partial production and loss rates as a function of atomic oxygen. For atomic oxygen concentrations greater than 8×10^9 cm^{-3} the increase of CO_3^- production is smaller than the increase of CO_3^- loss by atomic oxygen.

TABLE 4. Signal Flow Graph Characteristics for NO_3^- as a Function of Nitric Oxide Concentration at 65-km Altitude

n(NO), cm^{-3}	1×10^7	5×10^7	1×10^8	5×10^8
T_t	2.13	4.85	6.74	15.1
L	1.29×10^{-3}	1.34×10^{-3}	1.39×10^{-3}	1.80×10^{-3}
$\%_{77}$	17.4	21.2	21.6	22.3
g_{77}	2.09×10^{-6}	1.04×10^{-5}	2.10×10^{-5}	1.04×10^{-4}
Δ_{77}/Δ	1.78×10^5	9.87×10^4	7.05×10^4	3.24×10^4
T_{77}	0.372	1.03	1.48	3.38
$\%_{82}$	7.7	1.8	<1.0	<1.0
g_{82}	4.44×10^{-7}	4.42×10^{-7}	...	...
Δ_{82}/Δ	3.74×10^5	2.08×10^5	...	...
T_{82}	0.166	0.092	...	...
$\%_{102}$	48.5	59.3	60.9	62.4
g_{102}	2.78×10^{-6}	1.38×10^{-5}	2.78×10^{-5}	1.38×10^{-4}
Δ_{102}/Δ	3.74×10^5	2.08×10^5	1.48×10^5	6.82×10^4
T_{102}	1.04	2.88	4.11	9.43

6. Conclusion

In a study of *D* region ion chemistry the quantitative effect of any parameter can be analyzed in detail by applying *Mason's* [1956] rules to the corresponding signal flow graph. With these rules it is possible to evaluate quantitatively each production path and to know how each parameter influences the path gain or the amplification factor which is a measure of the chemical loops present in the system.

Negative ion clusters have been omitted in this paper, but any new reaction or new rate coefficient can be introduced in a straightforward manner. The major objective here is to present a tool appropriate to the analysis of large chemical systems under steady state conditions without transport effects. Nevertheless, the example at 65-km altitude clearly indicates significant variations of the negative ion concentrations as a function of adopted nitric oxide and atomic oxygen concentrations.

Appendix A: Signal Flow Graph and Mason's Rules

A graph is a set of nodes and edges which join two distinct nodes. The nodes in Figure 1 are the various negative ions and the edges are the oriented lines joining the ions. A path is composed by successive edges which never pass through the same node. A loop is a path for which the first node is identical to the last node. When numerical values are given to each edge, the value for a certain path or loop is simply the product of the values of the edges composing the path or the loop. These values are sometimes called path gains or loop gains.

Let us consider a system of k linear equations given by

$$x_i = \sum_{\substack{j=1 \\ j \neq i}}^{k} c_{ij} x_j + d_i \qquad \text{(A1)}$$

The flow graph associated with this system has the following characteristics: each unknown quantity x_i is associated with a node of the graph, each coefficient c_{ij} is the value of the edge oriented from j toward i, and the term d_i represents various external inputs to the system. The edge joining an input IN to a node always has a value equal to 1.

The system (A1) can be solved by classical methods. Such a procedure, however, gives no information on the relative importance of the various paths or loops in the associated graph. *Mason* [1956] developed a technique which expresses each unknown x_i of the system (A1) as a function of the various inputs and a quantity called transmittance, which depends on the values associated with the edges composing the graph. For m inputs IN corresponding to the values d_i in (A1), each unknown x_i is given [*Henley and Williams*, 1973] by

$$x_i = \sum_{j=1}^{m} T_{(i \leftarrow j)} \times (\mathrm{IN})_j \qquad \text{(A2)}$$

where the transmittance $T_{(i \leftarrow j)}$ is

$$T_{(i \leftarrow j)} = \sum_{l=1}^{n} g_l \Delta_l / \Delta \qquad \text{(A3)}$$

n being the number of paths joining the input $(IN)_j$ to the node i. In expression (A3), g_l is the numerical value (path gain) associated with each path joining the input j to the node i. The path gain g_l is always a product of edge values c_{ij}. The quantities Δ and Δ_l depend on the structure of the various loops in the graph; Δ is given by [*Mason*, 1956; *Henley and Williams*, 1973]

$$\Delta = 1 - \sum_1 + \sum_2 - \sum_3 + \cdots \quad \text{(A4)}$$

where $\sum_1$ is the sum of all loop gains in the graph, $\sum_2$ is the sum of products of all loop gains taken two at a time but excluding touching loops, and $\sum_3$ is the sum of products of all loop gains taken three at a time but excluding touching loops; Δ_l is obtained from Δ by deleting the loop gain terms touched by the lth path.

For a given input the transmittance is the product of g_l by Δ_l/Δ where g_l is the path gain and Δ_l/Δ is a factor resulting from all recycling loops existing in the graph. If there is no loop in the graph, Δ_l/Δ is equal to 1.

APPENDIX B: SIGNAL FLOW GRAPH AND ION CHEMISTRY IN THE D REGION

When transport processes are neglected, the steady state concentrations of positive (or negative) ions in the D region are obtained by equating production and loss terms for each ion. Furthermore, the electroneutrality condition can be used in a way such that the system of equations is linear. Mason's rules, described in Appendix A, are therefore directly applicable. Instead of writing a system of equations like (A1) in terms of concentrations it is more efficient to work with productions, since in this case the path gains have a real geophysical significance, as will be shown in this appendix.

For k negative ions including the electrons the production rate P_i (cm^{-3} s^{-1}) of the i type ion is given by

$$P_i = n_i L_i = \sum_{\substack{j=1 \\ j \neq i}}^{k} r_{ij} n_j + \gamma_i \quad \text{(B1)}$$

where L_i (in units per second) is the total loss rate of the i type ion with concentration n_i and γ_i is an external production rate (in cubic centimeters per second) which is zero for all negative ions and equal to γ_e for electrons. The coefficients r_{ij} can be considered as reaction rates in units per second which depend on the various rate coefficients, the neutral concentrations, and the positive ion concentrations.

System (B1) can also be written as

$$P_i = n_i L_i = \sum_{\substack{j=1 \\ j \neq i}}^{k} r_{ij}(L_j n_j / L_j) + \gamma_i \quad \text{(B2)}$$

or

TABLE B1. Reactions Used in an Oversimplified e-O_2^- System

Reaction	Rate Constant
$M + \text{photon or particle} \rightarrow e + M^+$	γ_e, cm^{-3} s^{-1}
$e + M^+ \rightarrow$ neutrals	α_1, cm^3 s^{-1}
$e + O_2 + M \rightarrow O_2^- + M$	k_1 cm^6 s^{-1}
$e + O_2 \rightarrow O_2^-$	k_2, cm^3 s^{-1}
$O_2^- + O \rightarrow e + O_3$	k_3, cm^3 s^{-1}
$O_2^- + O_2(^1\Delta_g) \rightarrow e + 2O_2$	k_4, cm^3 s^{-1}
$O_2^- + \text{photon} \rightarrow e + O_2$	J_1, s^{-1}
$O_2^- + M^+ \rightarrow$ neutrals	α_2, cm^3 s^{-1}

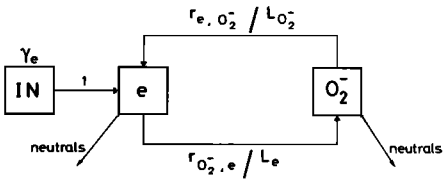

Fig. B1. Signal flow graph corresponding to the reactions of Table B1. All electron loss processes leading to O_2^- are combined under a single line from e to O_2^-. The line from O_2^- to e represents the three O_2^- loss processes of Table B1 giving rise to electrons. The input to the system is characterized by a production rate γ_e (cm^{-3} s^{-1}), and the path values are indicated on the line. Note that the value of the input line is 1.

$$P_i = \sum_{\substack{j=1 \\ j \neq i}}^{k} (r_{ij}/L_j) P_j + \gamma_i \quad \text{(B3)}$$

where P_j and L_j are the production rate (in cubic centimeters per second) and the total loss rate in units per second of the j type ion, respectively. The system of equations (B3) is formally identical to the system (A1), and Mason's rules (A2), (A3), and (A4) can be used to obtain the productions P_i in terms of inputs and transmittances. Knowing each production P_i, the individual concentrations n_i are obtained from $n_i = P_i/L_i$. Up to this point the signal flow graph gives exactly the same information as a classical solution, but the application of Mason's rules gives also the various transmittances indicating which physical process is important and how an input to the system is transferred to an ion through a specific path. Such an advantage is particularly rewarding when a large number of reactions are involved. Finally, the adoption of the production rate P_i as unknown leads to a simple interpretation of the terms r_{ij}/L_j which can be considered as relative loss rates. The coefficient r_{ij} is the loss rate of the j type ion toward i type ions, and L_j is the total loss rate of the j type ion.

Although a detailed proof is not simple, it has been shown [*Henley and Williams*, 1973] that Mason's rules lead to solutions of the system (A1) identical to results obtained from other methods. For comprehension of the signal flow graph technique we consider an oversimplified scheme of reactions involving only electrons and O_2^- ions as given in Table B1. When Mason's rules are applied to the corresponding system (B3), it is useful to check two points: (1) the solution obtained with Mason's rules is identical to the classical algebraic solution of system (B3); (2) the solution obtained with Mason's rules is identical to the solution obtained by equating electron or O_2^- production rates to their corresponding loss rates.

The signal flow graph is shown in Figure B1, where transitions from O_2^- to e and from e to O_2^- are represented by the top and bottom perimeters of the graph, respectively. This procedure is not mandatory, but it decreases significantly the total number of paths which have to be memorized in the graph analysis. The system (B3) reduces to

$$P_e = (r_{e,O_2^-}/L_{O_2^-}) P_{O_2^-} + \gamma_e \quad \text{(B4)}$$

and

$$P_{O_2^-} = (r_{O_2^-,e}/L_e) P_e \quad \text{(B5)}$$

The algebraic solutions of this system are

$$P_e = \gamma_e / [1 - (r_{e,O_2^-}/L_{O_2^-})(r_{O_2^-,e}/L_e)] \quad \text{(B6)}$$

and

$$P_{O_2^-} = \gamma_e (r_{O_2^-,e}/L_e) / [1 - (r_{e,O_2^-}/L_{O_2^-})(r_{O_2^-,e}/L_e)] \quad \text{(B7)}$$

According to Mason's rule (A2) and noting only one input IN $= \gamma_e$ in Figure B1, one obtains with $m = 1$

$$P_e = T_{(e\leftarrow 1)} \times \gamma_e \tag{B8}$$

and

$$P_{O_2^-} = T_{(O_2^-\leftarrow 1)} \times \gamma_e \tag{B9}$$

Since there is only one path joining the input γ_e to the node e or O_2^-, the transmittances $T_{(e\leftarrow 1)}$ and $T_{(O_2^-\leftarrow 1)}$ are given from (A3) as

$$T_{(e\leftarrow 1)} = g_1\Delta_1/\Delta \tag{B10}$$

$$T_{(O_2^-\leftarrow 1)} = g_1'\Delta_1'/\Delta \tag{B11}$$

For the electrons the path gain is $g_1 = 1$ along the path IN $\rightarrow$ e, and for O_2^-, the path gain is $g_1' = 1 \times (r_{O_2^-,e}/L_e)$ along the path IN $\rightarrow e \rightarrow O_2^-$. Since the graph in Figure B1 contains only one loop, (A4) leads to

$$\Delta = 1 - \sum_1 = 1 - (r_{e,O_2^-}/L_{O_2^-})(r_{O_2^-,e}/L_e) \tag{B12}$$

Since this sole loop touches the path IN $\rightarrow e$ and the path IN $\rightarrow e \rightarrow O_2^-$, one has $\Delta_1 = \Delta_1' = 1$. The transmittances (B10) and (B11) can finally be written as

$$T_{(e\leftarrow 1)} = 1/[1 - (r_{e,O_2^-}/L_{O_2^-})(r_{O_2^-,e}/L_e)] \tag{B13}$$

and

$$T_{(O_2^-\leftarrow 1)} = (r_{O_2^-,e}/L_e)/[1 - (r_{e,O_2^-}/L_{O_2^-})(r_{O_2^-,e}/L_e)] \tag{B14}$$

which lead with (B8) and (B9) to production rates identical to (B6) and (B7). Denoting a concentration by the corresponding chemical symbol in brackets, it can be seen from Table B1 that

$$L_e = k_1[O_2][M] + k_2[O_2] + \alpha_1[M^+] \tag{B15}$$

$$r_{O_2^-,e} = k_1[O_2][M] + k_2[O_2] \tag{B16}$$

$$L_{O_2^-} = k_3[O] + k_4[O_2(^1\Delta_g)] + J_1 + \alpha_2[M^+] \tag{B17}$$

and

$$r_{e,O_2^-} = k_3[O] + k_4[O_2(^1\Delta_g)] + J_1 \tag{B18}$$

where L_e and $L_{O_2^-}$ are the total loss rates in units per second for electrons and O_2^- ions, respectively; $r_{O_2^-,e}$ is the partial loss rate of electrons which are converted in O_2^-; and r_{e,O_2^-} is the partial loss rate of O_2^- ions which lead to electrons. The relative loss rates r_{ij}/L_j play the fundamental role in the transmittances. Substitution of (B15) to (B18) in the transmittances leads to production rates P_e and $P_{O_2^-}$, which, if divided by L_e and $L_{O_2^-}$, respectively, give electron and O_2^- concentrations identical to the classical result obtained without graph analysis.

The fundamental advantage of the application of Mason's rule is the access to the various transmittances which give a physical insight into the way in which a complicated system depends on some specific reactions. The term g_l in the transmittance gives the path gain toward a specific constituent when a path l is followed from the input. In other words, g_l measures the capacity of a specific path to transmit an external production. The term Δ_l/Δ is an amplification factor resulting from recycling processes. This factor measures the feedback mechanisms in the chemical system.

Acknowledgments. We are grateful to S. P. Zimmerman, T. J. Keneshea, and C. R. Philbrick for sending us numerical values for the neutral atmosphere model. The constructive comments of the anonymous referees are also appreciated.

The Editor thanks G. C. Reid for his assistance in evaluating this paper.

REFERENCES

Ackerman, M., In situ measurements of middle atmosphere composition, *J. Atmos. Terr. Phys., 41,* 723–733, 1979.

Albritton, D. L., Ion-neutral reaction-rate constants measured in flow reactors through 1977, *At. Data Nucl. Data Tables, 22,* 1–101, 1978.

Arijs, E., J. Ingels, and D. Nevejans, Mass spectrometric measurement of the positive ion composition in the stratosphere, *Nature, 271,* 642–644, 1978.

Arnold, F., and G. Henschen, First mass analysis of stratospheric negative ions, *Nature, 275,* 521–522, 1978.

Arnold, F., J. Kissel, D. Krankowsky, H. Wieder, and J. Zähringer, Negative ions in the lower ionosphere: A mass-spectrometer measurement, *J. Atmos. Terr. Phys., 33,* 1167–1175, 1971.

Arnold, F., H. Böhringer, and G. Henschen, Composition measurements of stratospheric positive ions, *Geophys. Res. Lett., 5,* 653–656, 1978.

Cosby, P. C., J. H. Ling, J. R. Peterson, and J. T. Moseley, Photodissociation and photodetachment of molecular negative ions, III, Ions formed in $CO_2/O_2/H_2O$ mixtures, *J. Chem. Phys., 65,* 5267–5274, 1976.

Ferguson, E. E., Laboratory measurements of ionospheric ion-molecule reaction rates, *Rev. Geophys. Space Phys., 12,* 703–713, 1974.

Ferguson, E. E., D. B. Dunkin, and F. C. Fehsenfeld, Reaction of NO_2^- and NO_3^- with HCl and HBr, *J. Chem. Phys., 57,* 1459–1463, 1972.

Goldberg, R. A., and A. C. Aikin, Studies of positive ion composition in the equatorial *D* region ionosphere, *J. Geophys. Res., 76,* 8352–8364, 1971.

Goldberg, R. A., and L. J. Blumle, Positive ion composition from a rocket-borne mass spectrometer, *J. Geophys. Res., 75,* 133–142, 1970.

Henley, E. J., and R. A. Williams, *Graph Theory in Modern Engineering, Math. in Sci. and Eng.,* vol. 98, Academic, New York, 1973.

Huang, C.-M., M. Whitaker, M. A. Biondi, and R. Johnsen, Electron-temperature dependence of recombination of electrons with $H_3O^+ \cdot (H_2O)_n$-series ions, *Phys. Rev. A, 18,* 64–67, 1978.

Johannessen, A., and D. Krankowsky, Positive-ion composition measurement in the upper mesosphere and lower thermosphere at high latitude during summer, *J. Geophys. Res., 77,* 2888–2901, 1972.

Keesee, R. G., N. Lee, and A. W. Castleman, Jr., Atmospheric negative ion hydration derived from laboratory results and comparison to rocket-borne measurements in the lower ionosphere, *J. Geophys. Res., 84,* 3719–3722, 1979.

Keneshea, T. J., S. P. Zimmerman, and C. R. Philbrick, A dynamic model of the mesosphere and lower thermosphere, *Planet. Space Sci., 27,* 385–401, 1979.

Lee, L. C., and G. P. Smith, Photodissociation and photodetachment of molecular negative ions, III, Ions in $O_2/CH_4/H_2O$ mixtures from 3500 to 8600 Å, *J. Chem. Phys., 70,* 1727–1735, 1979.

Mason, S. J., Feedback theory—Further properties of signal flow graphs, *Proc. IRE, 44,* 920–926, 1956.

Mul, P. M., and J. W. McGowan, Merged electron-ion beam experiments, III, Temperature dependence of dissociative recombination for atmospheric ions NO^+, O_2^+, and N_2^+, *J. Phys. B,* 1591–1601, 1979.

Narcisi, R. S., Ion composition of the mesosphere, *Space Res., 7,* 186–196, 1967.

Narcisi, R. S., and A. D. Bailey, Mass spectrometric measurements of positive ions at altitudes from 64 to 112 kilometers, *J. Geophys. Res., 70,* 3687–3700, 1965.

Narcisi, R. S., A. D. Bailey, L. Della Luca, C. Sherman, and D. M. Thomas, Mass spectrometric measurements of negative ions in the *D*- and lower *E*-regions, *J. Atmos. Terr. Phys., 33,* 1147–1159, 1971.

Narcisi, R. S., A. D. Bailey, L. E. Wlodyka, and C. R. Philbrick, Ion composition measurements in the lower ionosphere during the November 1966 and March 1970 solar eclipses, *J. Atmos. Terr. Phys., 34,* 647–658, 1972.

Phelps, A. V., Laboratory studies of electron attachment and detach-

ment processes of aeronomic interest, *Can. J. Chem., 47,* 1783–1793, 1969.
Reid, G. C., Physical processes in the *D* region of the ionosphere, *Rev. Geophys. Space Phys., 2,* 311–333, 1964.
Reid, G. C., Ion chemistry in the *D* region, in *Advan. At. Mol. Phys.,* vol. 12, edited by D. R. Bates and B. Bederson, pp. 375–413, Academic, New York, 1976.
Smith, D., N. G. Adams, and M. J. Church, Mutual neutralization rates of ionospherically important ions, *Planet. Space Sci., 24,* 697–703, 1976.
Smith, E. V. P., and D. M. Gottlieb, Solar flux and its variations, *Space Sci. Rev., 16,* 771–802, 1974.
Smith, G. P., and L. C. Lee, Photodissociation of atmospheric positive ions, II, 3500–8600 A, *J. Chem. Phys., 69,* 5393–5399, 1978.
Smith, G. P., L. C. Lee, P. C. Cosby, J. R. Peterson, and J. T. Moseley, Photodissociation and photodetachment of molecular negative ions, V, Atmospheric ions from 7000 to 8400 Å, *J. Chem. Phys., 68,* 3818–3822, 1978.
Stelman, D., J. L. Moruzzi, and A. V. Phelps, Low energy electron attachment to ozone using swarm techniques, *J. Chem. Phys., 56,* 4183–4189, 1972.
Swider, W., Aeronomic aspects of the polar *D*-region, *Space Sci. Rev., 20,* 69–114, 1977.
Thomas, L., Recent developments and outstanding problems in the theory of the *D* region, *Radio Sci., 9,* 121–136, 1974.
Thomas, L., P. M. Gondhalekar, and M. R. Bowman, The influence of negative-ion changes in the *D*-region during sudden ionospheric disturbances, *J. Atmos. Terr. Phys., 35,* 385–395, 1973*a*.
Thomas, L., P. M. Gondhalekar, and M. R. Bowman, The negative-ion composition of the daytime *D*-region, *J. Atmos. Terr. Phys., 35,* 397–404, 1973*b*.
Truby, F. K., Low-temperature measurements of the three-body electron-attachment coefficient in O_2, *Phys. Rev. A, 6,* 671–676, 1972.
Turco, R. P., A discussion of possible negative ion detachment mechanisms in the sunrise *D* region, *Radio Sci., 9,* 655–658, 1974.
Turco, R. P., and C. F. Sechrist, Jr., An investigation of the ionospheric *D* region at sunrise, *Aeron. Rep. 41,* Aeron. Lab., Univ. of Ill., Urbana-Champaign, 1970.
Turco, R. P., and C. F. Sechrist, Jr., An investigation of the ionospheric *D* region at sunrise, 2, Estimation of some photodetachment rates, *Radio Sci., 7,* 717–723, 1972*a*.
Turco, R. P., and C. F. Sechrist, Jr., An investigation of the ionospheric *D* region at sunrise, 3, Time variations of negative-ion and electron densities, *Radio Sci., 7,* 725–737, 1972*b*.
Zbinden, P. A., M. A. Hidalgo, P. Eberhardt, and J. Geiss, Positive ion composition in the lower ionosphere during the Geminid meteor shower and the occurrence of a winter anomaly, in *Methods of Measurements and Results of Lower Ionosphere Structure,* edited by K. Rawer, pp. 281–286, Akademie-Verlag, Berlin, 1974.
Zbinden, P. A., M. A. Hidalgo, P. Eberhardt, and J. Geiss, Mass spectrometer measurements of the positive ion composition in the *D*- and *E*-regions of the ionosphere, *Planet. Space Sci.,* 1621–1642, 1975.

(Received January 22, 1980;
revised March 19, 1980;
accepted April 9, 1980.)